Sound & Vibration 2026, 60(5), 4326.
doi: https://doi.org/10.59400/sv4326

Article

Study on the vibration transmission speed and damping characteristics of piano soundboard

Jinyi Chen, Guanzheng Wan, Lan He, Jing Zhou, Haotian Cui, Zhenbo Liu*

Key Laboratory of Bio-Based Material Science & Technology of Ministry of Education, Northeast Forestry University, Harbin 150040, China
*** Corresponding author:** Zhenbo Liu, liu.zhenbo@foxmail.com

CITATION

Chen J, Wan G, He L, et al. Study on the vibration transmission speed and damping characteristics of piano soundboard. Sound & Vibration. 2026; 60(5): 4326. https://doi.org/10.59400/sv4326

ARTICLE INFO

Received: 26 April 2026
Revised: 17 May 2026
Accepted: 27 May 2026
Available online: 23 July 2026

Abstract: The piano soundboard converts string vibrations into radiated sound, affecting tonal quality. However, the propagation and energy dissipation of vibration waves along different grain directions remain insufficiently studied. To study vibration wave propagation and dissipation in piano soundboards of different composite processes, four quarter-size soundboards (moisture content 7%–9%) were selected: one tone-wood soundboard (T) and three laminated boards (L90 with vertical core, L55 with inclined core, L180 with horizontal core). Free boundary conditions were simulated via elastic rope suspension; time-domain responses were recorded at 16 kHz sampling (2,048 points). The angle α between the line connecting the two accelerometers and the core layer direction (for T, grain direction defined as 0°) was varied from 0° (parallel) to 90° (perpendicular) in 15° steps. Wave velocity and damping ratios were extracted using gradient and envelope fitting methods. The results showed: T exhibited the highest wave velocity from 0° to 90°, decreasing with angle (R^2 = 0.985), and a maximum anisotropy ratio of 4.59; L90 was angle-insensitive with weak correlation (R^2 = 0.735); L55 showed a trend similar to T (R^2 = 0.990); the wave velocity of L180 generally decreased but rebounded at 30°. Broadband damping ratios were 0.002–0.007, with T averaging 0.0040 (maximum 0.0058), L90 the lowest (average 0.0035, maximum 0.0049), L55 the highest (average 0.0051, maximum 0.0065), and L180 averaging 0.0038 (maximum 0.0062). Narrowband analysis showed that the damping ratios of all soundboards decreased exponentially with increasing frequency. The results guide piano soundboard vibration, material selection, and processing.

Keywords: four types of piano soundboards; wave velocity; damping ratio; different grain directions; frequency dependence

1. Introduction

The piano is hailed as the "king of instruments"; the quality of its sound largely depends on the vibration response characteristics of the soundboard [1]. As the most important sound-radiating component in the piano structure, the soundboard performs the core function of converting the vibration energy of the strings into sound energy and radiating it outward. After the keys are struck, the vibration of the strings is transmitted to the soundboard through the bridge, exciting the soundboard to produce bending waves. The vibration energy then spreads from the point of excitation across the entire board, eventually radiating sound through the board's vibrations. Therefore, the vibration behavior of the soundboard directly determines key acoustic indicators of the piano, such as loudness, timbre, sustain, and transient response.

Spruce has become nearly the sole choice for soundboards due to its combination of light weight, high strength, high wave velocity, and moderate internal damping [2]. Its significant orthotropic anisotropy makes the elastic modulus along the grain 10 to 20 times higher than that across the grain [3]. This characteristic causes the propagation of vibration waves in the soundboard to exhibit obvious directional dependence: propagation is faster along the grain and slower across the grain [2, 4]. At the same time, as a natural polymer material, wood's internal damping characteristics lead to the gradual dissipation of vibration energy, directly affecting the sustain length and spectral decay characteristics of the piano [5, 6]. It can be seen that wave velocity [7], anisotropy [7–9], and damping ratio [10, 11] are three fundamental parameters describing the vibration response characteristics of a piano soundboard. Wave velocity determines the speed of vibration energy diffusion, anisotropy reflects the directional preference of energy propagation, and the damping ratio controls the rate of energy dissipation. The three are interrelated and together shape the vibration response behavior of the soundboard.

In the study of vibration characteristics, both theoretical and experimental researchers worldwide have conducted extensive work focusing on three fundamental parameters: wave velocity, anisotropy, and damping. At the theoretical level, the classical thin-plate bending theory provides a basic framework for analyzing the wave propagation behavior of orthotropic plates, giving a theoretical relationship between the ratio of elastic moduli in the longitudinal and transverse directions and the square of the wave velocity, thus providing a basis for deducing the elastic modulus ratio through wave velocity measurements [12]. For the measurement of wave velocity and elastic modulus, commonly used methods include the ultrasonic pulse method [13, 14], the dynamic suspension method, the time-of-flight method using a sound velocity meter, and the impact resonance method based on FFT spectral analysis [15]. Among these, the spectral analysis method based on free vibration can simultaneously determine the bending stiffness, dynamic elastic modulus, and longitudinal wave velocity of the resonant plate. Urgela proposed using holographic interferometry (TV holography and double-pulse laser holography) to visualize standing waves and transient waves in wooden plates. Based on the theory of bending waves in orthotropic plates, this method allows non-destructive estimation of the longitudinal and tangential Young's moduli and in-plane shear modulus, suitable for material grading and selection for pianos and bowed string instruments [16]. Zhang et al. measured the wave velocity of spruce wood used for pianos using the dynamic suspension method and the sound velocity method, respectively. The results of the two methods were very close, with a relative error of only 1.2%, within the permissible engineering range [17]. In terms of damping characteristics, modal analysis and narrowband filtering methods are classical techniques for obtaining modal damping ratios and are often used to measure the modal frequencies and modal damping, and mode shapes of piano soundboards [18]. Miao et al. explored the influence of resonant plate vibration characteristics on piano timbre using the FFT spectral analysis method and found that with the increase of elastic modulus and wave velocity, the acoustic quality of the piano correspondingly improved. Georges used experimental modal analysis techniques to obtain the bending vibration characteristics of wooden beam components under free-support conditions through hammer excitation, and extracted the frequency, damping ratio, and mode shape of each mode, determined the anisotropic Young's modulus and other dynamic mechanical properties of the wood, and verified the effectiveness of this method using static four-point bending tests [19].

However, existing studies exhibit significant limitations in multiple aspects. Firstly, in terms of damping parameter extraction, most works employ narrowband filtering or modal decomposition methods, which face major challenges when dealing with multi-modal superimposed responses. In a piano soundboard under actual operating conditions, neighboring modal frequencies are close to each other, leading to significant modal interference and spectral aliasing phenomena. Narrowband filtering requires truncating specific modes in the frequency domain to obtain approximate single-mode responses, but this operation inevitably loses information about the dynamic energy exchange between modes and the relative phase information between them. More critically, when the natural frequencies of adjacent modes are too close, frequency-domain separation cannot achieve effective isolation, and the aliasing errors thus produced cause the identified damping ratios to deviate from their true values. In fact, numerous studies have confirmed that narrowband filtering methods struggle to accurately identify damping parameters in multi-modal systems, and the errors generated thereby exhibit systematic characteristics [20]. Secondly, in terms of wave velocity and anisotropy measurement, traditional methods such as cross-correlation or phase difference methods require high signal purity and signal-to-noise ratio, and their reliability degrades markedly when faced with multi-modal superimposed responses [21]. These methods typically assume that the analyzed signal is an ideal waveform of a single propagation mode, whereas under actual soundboard conditions, the superposition of wave components from different modes means that a single measurement channel often receives a coupled result of multiple wave packets, making cross-correlation results vulnerable to interference and susceptible to measurement deviation. As wood is a natural polymer material, the inhomogeneity of its internal structure further complicates wave propagation analysis. Moreover, characterizing the orthotropic anisotropy and viscoelastic mechanical behavior of wood over a broad frequency range requires considering both frequency-dependent propagation and dissipation mechanisms, which poses severe challenges for traditional narrowband excitation experimental methods.

Faced with the inherent limitations of narrowband filtering in dense modal systems, this study introduces the envelope method as a strategy for extracting equivalent damping ratios. The core advantages of the envelope method are reflected in the following aspects. Firstly, the envelope method does not rely on frequency-domain modal separation but directly processes vibration decay signals in the time domain, extracting equivalent damping characteristics from the overall decay envelope, thereby avoiding modal information fragmentation and phase information loss caused by frequency-domain segmentation. Secondly, the envelope method can effectively handle non-exponential decay problems caused by modal overlap by directly analyzing the upper envelope of the time-domain signal or using the Hilbert transform to obtain the signal's complex analytic representation, extracting the overall energy decay rate while retaining inter-modal coupling information; the resulting damping ratios are closer to the effective damping characteristics under actual operating conditions. Moreover, through the combined use of the Hilbert transform and empirical mode decomposition, both instantaneous envelope and instantaneous phase information can be obtained from free vibration decay signals, enabling the derivation of the system's global damping parameters from the logarithmic decay rate of the envelope. This time-domain identification method also demonstrates high accuracy and noise resistance in nonlinear system parameter identification. Existing studies have shown that the Hilbert–Huang transform (HHT), which combines empirical mode decomposition, can identify the modal frequencies and damping ratios of multi-degree-of-freedom systems. During the decomposition process, constructing internal local symmetric mean lines through pole symmetry can effectively reduce interpolation uncertainty.

In response to the aforementioned shortcomings, the core innovative contributions of this work are reflected in the following three aspects: First, a damping ratio extraction strategy that does not require narrowband filtering is proposed, which directly uses the envelope method to extract the equivalent damping ratio from the original broadband time-domain response, fully retaining modal coupling information and avoiding systematic deviations in damping estimation. Second, a comprehensive evaluation framework for wave velocity, anisotropy, and damping ratio on the same specimen and under identical conditions is established, revealing the synergistic effects of the three on the propagation and dissipation of vibrational energy in the soundboard. Third, this work provides directly applicable equivalent damping ratio data to support material selection and acoustic optimization of piano soundboards. In this study, vibration signal analysis (gradient method for wavefront identification, Hilbert envelope extraction of damping ratio, etc.) was used to measure the wave velocity, anisotropy, and damping characteristics of four types of piano soundboards (tone-wood soundboard T, laminate soundboard with vertical core L90, laminate soundboard with incline core L55, laminate soundboard with horizontal core L180) at different grain angles, and the frequency dependence of the damping ratio was analyzed. The results address the issues of inaccurate wave velocity extraction under multimodal superposition and the difficulty of directly correlating parameters when wave velocity, anisotropy, and damping ratio are measured separately on different soundboards and under different conditions. In addition, it was found that a decoupling between stiffness (wave velocity) and damping mechanisms exists in laminated structures, providing an experimental basis for material selection and acoustic optimization of piano soundboards.

2. Materials and methods

2.1. Experimental materials

This study focuses on upright piano soundboards made with four different composite processes (two per type, for a total of eight samples) manufactured by Chengdu CANYA Wood Industry Co., Ltd. (Chengdu, China). These four structures are currently the most commonly used soundboard types in pianos. For ease of measurement, the dimensions of the soundboards are one quarter of those of actual piano products. The top plate and core board are made of quarter-sawn spruce with fish-scale figure. The soundboards were conditioned at room temperature to a moisture content of 7–9%. **Figure 1** shows the structures of the four piano soundboards and the grain direction of each component, and **Table 1** lists the composite types and parameters.

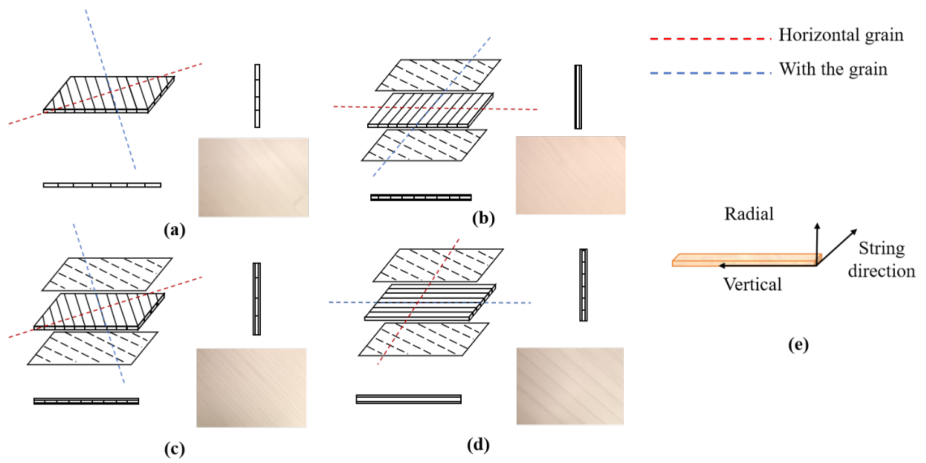

Figure 1. Four types of piano soundboard structures: **(a)** Tone-wood soundboard; **(b)** Laminate soundboard with vertical core; **(c)** Laminate soundboard with incline core; **(d)** Laminate soundboard with horizontal core; **(e)** The wood direction of the units.

Table 1. Composite conditions and basic parameters of piano soundboards.

Sample group	Type	Core	Angles of the surface layer to the cores	Dimensions (mm)	Density ($kg \cdot m^{-3}$)
T	tone-wood soundboard	-	47°	697.93 × 497.77 × 9.22	460.45
L90	laminate soundboard	vertical core	90°/45°	695.25 × 496.83 × 7.39	450.87
L55	laminate soundboard	incline core	55°/42°	697.17 × 496.92 × 8.43	462.51
L180	laminate soundboard	horizontal core	180°/45°	700.51 × 496.83 × 8.04	455.45

2.2. Experimental methods

Figure 2 shows the system used to measure the free vibration of the soundboard. The specimen was suspended using elastic cords (cross-suspended at the centerlines of the specimen’s length and width) to maintain a free boundary condition. A multi-channel dynamic signal acquisition and analysis instrument (ZS7016, Yangzhou Zhongsheng Technology Co., Ltd., Yangzhou, China) was used. The excitation was applied via a blade, and the vibration signals were collected by an accelerometer and transmitted to the dynamic signal acquisition and analysis software to obtain the time-domain responses of the specimen.

Taking the laminate soundboard with a horizontal core as an example, the arrangement of the two accelerometers in the experiment is shown in **Figure 3**. Two concentric circles are drawn with the excitation point as the origin. The radial distance between the two concentric circles should be large enough, and the sampling frequency should be high enough to ensure detection of the time difference between the two signals. In this experiment, the radial distance between the two accelerometers was set to 300 mm, the sampling frequency was set to 16,000 Hz, and the number of sampling points was 2,048. The angle α between the line connecting the two accelerometers and the grain direction of the core layer was varied from 0° (parallel) to 90° (perpendicular) in 15° increments.

Figure 2. Measuring system with cross-suspension support and the positions of excitation and the accelerometer.

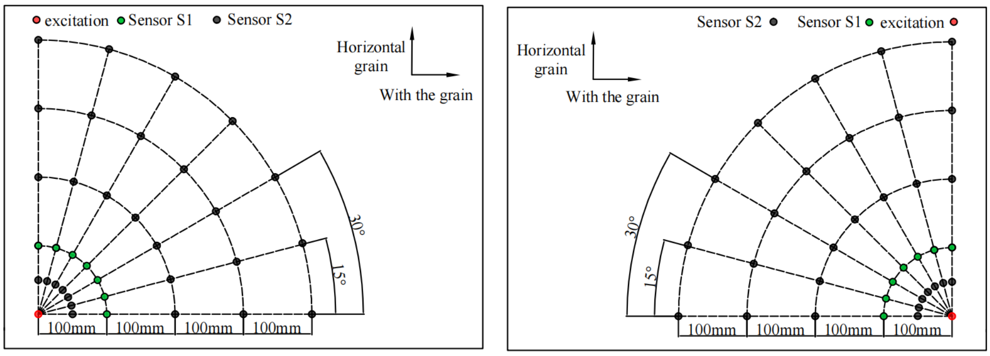

Figure 3. Schematic diagram of measurement points on the laminate soundboard with a horizontal core.

2.3. Determination of vibration wave velocity in piano soundboards using the gradient method

The propagation characteristics of vibrations in the piano soundboard are one of the key factors determining its acoustic quality. The wavefront, as the moment when vibrational energy first reaches a certain point in space, directly reflects the diffusion rate and anisotropic characteristics of energy on the soundboard. By analyzing the wavefront arrival times at different positions, the wave velocity can be quantitatively obtained, thereby revealing the vibration propagation mechanism of the soundboard. In this study, a gradient method was used to extract the wavefront moment: first, the signal was smoothed, and then its first-order derivative was calculated; using a threshold of three times the standard deviation of the noise (above the noise mean), the first positive peak was detected as the wavefront moment (**Figure 4**). Two accelerometers were arranged linearly along the propagation direction, and the wave velocity was calculated using Equation (1) [12]:

$$v = \frac{d}{t_2 - t_1}, \tag{1}$$

where d is the distance between the two accelerometers, and t_1 and t_2 are the wavefront moments at accelerometers S1 and S2, respectively.

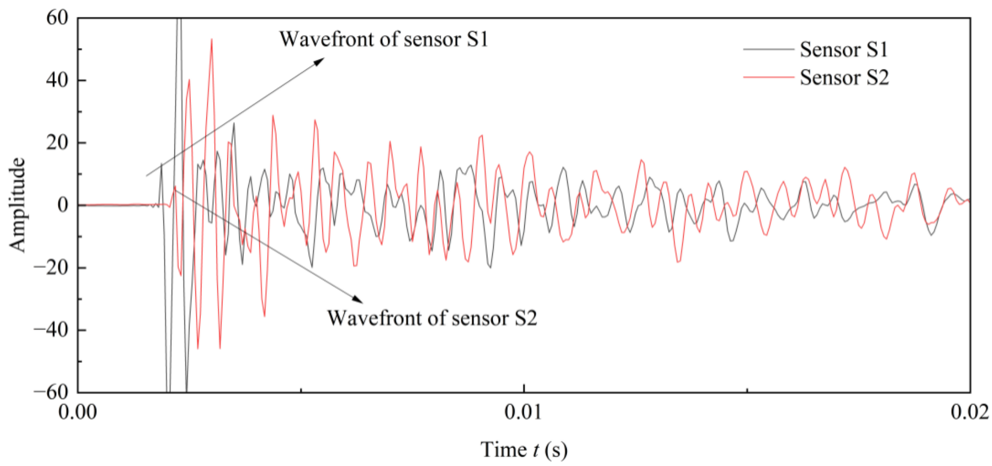

Figure 4. Schematic of the wavefront moments detected by the two accelerometers.

2.4. Determination of anisotropy based on thin-plate bending theory

Anisotropy is an important indicator for describing the differences in the elastic modulus of wood. Due to the pronounced directionality and regularity of structural factors such as the shape and arrangement of wood cells and the orientation of the cellulose fibrils in the S_2 layer of the cell wall, the elastic modulus and wave velocity of wood vary along the three principal axes, with the difference between the longitudinal and transverse directions being the most significant. For a wood specimen of a given density, the relationship between elastic modulus and propagation velocity can be expressed as Equation (2) [22]:

$$\sqrt{\frac{E_{\parallel}}{E_{\perp}}} = \frac{v_{\parallel}}{v_{\perp}} = \frac{v_0}{v_{90}}, \tag{2}$$

where v_0 is the wave velocity along the grain, and v_{90} is the wave velocity across the grain.

This ratio reflects the directional differences in material stiffness: the larger the ratio, the more obvious the anisotropy; the closer the ratio is to 1, the more the material tends to be isotropic.

2.5. Determination of damping ratio based on the envelope fitting method

Damping is a parameter that characterizes energy dissipation in a structural system during vibration. It essentially represents the conversion of vibrational energy—specifically, the process by which mechanical energy is transformed into heat or other forms of energy [23]. In this study, the damping ratio was extracted from the measured free decay signals using the envelope fitting method based on the Hilbert transform. This method extracted the amplitude envelope from the analytic signal and used data from the entire decay segment for least squares fitting, allowing for a more robust estimation of the decay coefficient [24]. In addition, the linearity of the logarithmic envelope plot can directly verify the applicability of the viscous damping model, providing an intuitive basis for the correctness of damping analysis. Therefore, the envelope fitting method is more suitable for handling vibration signals of complex structures such as soundboards.

The signal envelope $E(t)$ is extracted via the Hilbert transform, and its natural logarithm is taken, as shown in Equations (3) and (4) [25]:

$$lnE(t) = lnA - \zeta\omega_n t, \tag{3}$$

$$\zeta = -\frac{k}{\omega_n}. \tag{4}$$

A linear least-squares fit of $lnE(t)$ was then performed within the selected decay segment to obtain the slope $k = -\zeta\omega_n$. Combining this slope with ω_n obtained from the peak intervals or the frequency spectrum, the damping ratio can be determined. This method tolerates noise to a certain extent and makes it possible to visually verify whether the decay conforms to an exponential law [26].

2.6. Determination of relative node energy based on wavelet packet decomposition

Traditional wavelet decomposition only performs layer-by-layer decomposition of the low-frequency approximation components, while the high-frequency detail components are not further decomposed, which results in poor frequency resolution at high frequencies. Wavelet packet decomposition overcomes this limitation by decomposing all nodes at each level (including both approximation and detail), thereby forming a complete binary tree structure [27]. This decomposition method can adaptively select frequency bands based on the signal characteristics, revealing the time-frequency features of the signal more comprehensively.

For a one-dimensional signal, wavelet packet decomposition divides the signal layer by layer into multiple subbands, each corresponding to a specific frequency band. A higher number of decomposition layers yields higher frequency resolution. Each node corresponds to a specific frequency subband and carries the corresponding wavelet packet coefficients.

The sampling frequency during the test was 16,000 Hz, so the Nyquist frequency was 8,000 Hz. After wavelet packet decomposition, the bandwidth of each subband at the third level was 1,000 Hz. That is, the signal was analyzed within the frequency bands shown in **Table 2**.

Table 2. Frequency ranges corresponding to signal nodes at the third level of decomposition.

Signal node	Frequency range/Hz	Signal node	Frequency range/Hz
1	0–1,000	5	4,000–5,000
2	1,000–2,000	6	5,000–6,000
3	2,000–3,000	7	6,000–7,000
4	3,000–4,000	8	7,000–8,000

For the i-th node in the j-th layer after decomposition, its energy is defined as the sum of the squares of its wavelet packet coefficients, as shown in Equation (5) [28]:

$$E_{j,i} = \sum_{k=1}^{N} |C_{j,i}(k)|^2, \tag{5}$$

where $C_{j,i}(k)$ is the k-th coefficient of the node, and N is the total number of coefficients. This energy reflects the signal strength within this frequency band.

To compare the relative contributions among different frequency bands, the energy is normalized to relative energy, as shown in Equation (6) [28]:

$$P_{j,i} = \frac{E_{j,i}}{\sum_i E_{j,i}}. \tag{6}$$

3. Results and discussion

3.1. Vibration wave velocity in piano soundboards

To accurately determine the vibration wave velocity in piano soundboards and investigate the effect of propagation direction on wave velocity, this study varies the angle α between the sensor axis and the core layer direction from 0° to 90° in 15° increments on each sample. Broadband response signals are obtained via single-point excitation and two accelerometers, and wave velocities in each direction are extracted using the gradient method.

As shown in **Table 3**, T (tone-wood soundboard), L55 (laminate soundboard with an incline core), and L180 (laminate soundboard with a horizontal core) generally follow the pattern that wave velocity decreases as the grain angle increases. However, the wave velocity of L90 (laminate soundboard with vertical core) is not sensitive to changes in grain angle. Over the range 0°–75°, the maximum difference in wave velocity for L90 is only 70.81 m/s, which is much smaller than that observed for the other soundboards.

Table 3. Vibration wave velocity in different directions of the piano soundboard.

Angle α/°	Distance d/mm	T		L90		L55		L180	
		Time difference/ms	Wave velocity/m·s^{-1}	Time difference/ms	Wave velocity/m·s^{-1}	Time difference/ms	Wave velocity/m·s^{-1}	Time difference/ms	Wave velocity/m·s^{-1}
0	300	0.294	1,033.33	0.395	588.52	0.382	797.83	0.420	740.97
15	300	0.402	841.59	0.566	559.49	0.503	712.91	0.498	634.22
30	300	0.401	762.68	0.625	519.85	0.430	698.65	0.472	667.56
45	300	0.450	670.21	0.622	528.68	0.486	628.39	0.548	556.33
60	300	0.537	570.28	0.619	535.18	0.595	530.16	0.619	524.40
75	300	0.557	564.92	0.713	517.71	0.639	484.75	0.828	369.59
90	300	0.636	482.46	0.997	306.79	0.757	398.20	0.911	359.39

T (tone-wood soundboard): The wave velocity decreases monotonically with increasing grain angle, dropping from 1,033 m/s to 482 m/s. The downward trend is smooth, without significant fluctuations, which aligns with the typical rules of orthotropic anisotropy in wood. This is because spruce is composed of tracheids arranged axially, with cellulose microfibrils in the cell walls almost parallel along the axis, providing extremely high specific elastic modulus in the longitudinal direction, while in the transverse direction, it relies only on wood rays, the middle lamella between cell walls, and hemicellulose connections [29].

L90 (laminate soundboard with vertical core): Over the range 0°–75°, the wave velocity fluctuates between 517 and 589 m/s. The values at 45° (528.68 m/s) and 60° (535.18 m/s) are higher than those at 30°, showing no clear monotonic trend. The wave velocity then drops sharply to 307 m/s at 90°, yielding an irregular overall pattern.

L55 (laminate soundboard with incline core): The wave velocity decreases monotonically, dropping from 798 m/s to 398 m/s, with a smooth curve, similar to that of T, but with a slightly smaller decline.

L180 (laminate soundboard with horizontal core): Overall, L180 shows a downward trend, but the wave velocity at 30° (667.56 m/s) is higher than that at 15° (634.22 m/s), showing a local rebound that indicates some degree of variability.

In addition, T generally exhibits higher wave velocities than the laminate soundboards across all measured angles. This is because the grain angle between the top and core boards of laminate soundboards significantly reduces the overall bending stiffness, and the glue layer and the interlayer interface disrupt the continuity of stress transfer. Although laminate soundboards still exhibit directionality, the cross-laminated structure weakens the anisotropy, reducing the angle sensitivity of the wave velocity.

The relationship between wave velocity and grain angle was analyzed (**Figure 5**), and a quadratic polynomial was fitted using the least squares method, yielding:

$$\text{T: } v_1(\alpha) = 0.05\alpha^2 - 9.99\alpha + 1{,}014.10, \tag{7}$$

$$\text{L90: } v_2(\alpha) = -0.04\alpha^2 + 1.65\alpha + 558.08, \tag{8}$$

$$\text{L55: } v_3(\alpha) = -0.01\alpha^2 - 3.30\alpha + 789.58. \tag{9}$$

$$\text{L180: } v_4(\alpha) = -0.02\alpha^2 - 2.90\alpha + 727.23, \tag{10}$$

Equations (7)–(9) can be summarized as:

$$v(\alpha) = A\alpha^2 + B\alpha + C, \tag{11}$$

where $v(\alpha)$ is the wave velocity at an angle α relative to the grain direction, $v(0)$ is the wave velocity along the grain, $v(90)$ is the wave velocity across the grain, and A, B, C are the constants obtained from the regression of wave velocity against grain angle.

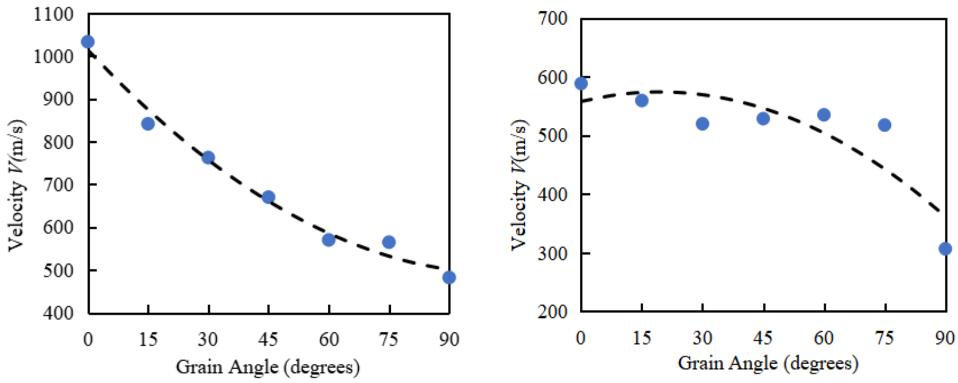

(a) **(b)**

Figure 5. *Cont.*

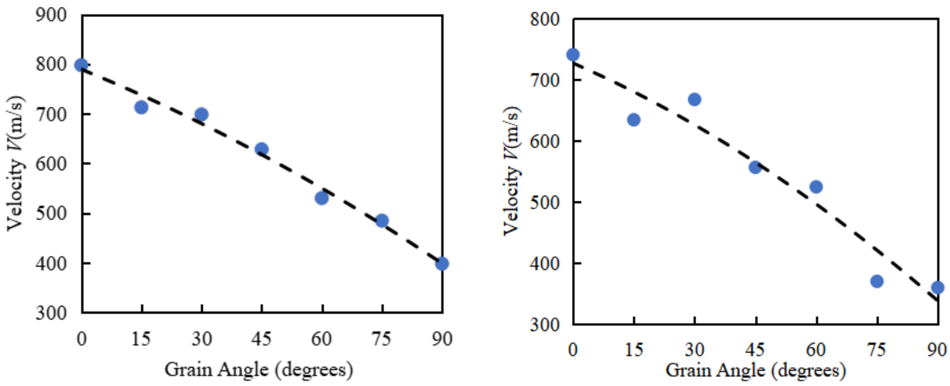

(c) (d)

Figure 5. The relationship between wave velocity (V) and grain angle: **(a)** Tone-wood soundboard; **(b)** Laminate soundboard with vertical core; **(c)** Laminate soundboard with incline core; **(d)** Laminate soundboard with horizontal core.

As can be seen from **Table 4** and **Figure 5**, the fitting curves for T (tone-wood soundboard) and L55 (laminate soundboard with an incline core) both have R^2 values above 0.95, indicating that the goodness of fit is excellent. L180 (laminate soundboard with horizontal core) has R^2 = 0.937, which is a good fit and within the acceptable range in engineering. L90 (laminate soundboard with vertical core) is relatively poor, with a value of only 0.735. This may be due to differences in soundboard structures. T is made of natural wood, with continuous fibers and significant anisotropy. The wave velocity varies with angle strictly following the orthotropic anisotropy theory of wood. Since there is no interface interference, the measurement data are stable, and the fitting effect is excellent. In contrast, the structure of laminate soundboards is fundamentally different from that of a tone-wood soundboard: laminate soundboards usually consist of a high-quality solid wood face layer (such as spruce) and a core board made by splicing radially cut veneers. This structure disrupts the continuity of wave propagation in an ideal orthotropic anisotropic panel, weakening the material's anisotropy. When the face layer is bonded to the core board, the mechanical properties of the face layer can reduce the overall anisotropy [30]. Thus, although the wave velocities at 0° (along the grain) and 90° (across the grain) differ, the wave velocities at intermediate angles (e.g., 15° and 30°) may not show any regular pattern due to the stiffness contribution of the face layer.

Table 4. Root-mean-square error (RMSE) and coefficient of determination (R^2) for polynomial fitting.

Sample group	RMSE	R^2
T	21.45	0.985
L90	43.98	0.735
L55	15.02	0.990
L180	33.72	0.937

In addition, the adhesive layers in composite structures [31] and the interfaces between different materials [32] can also cause strong scattering of vibration waves [7,33]. When the angle between the sensor axis and the grain direction is varied, the actual propagation path of the wave may no longer be straight, but rather a complex path that bypasses or penetrates different materials, resulting in random fluctuations in the measured wave velocity [34].

This variability reflects the complexity of the laminated structure. Due to the stiffness contribution of the face layer and the scattering effect of the interlayer interfaces, the wave velocity of the laminate soundboard is less sensitive to changes in angle than that of a tone-wood soundboard, and its fluctuating behavior no longer strictly follows that of the ideal orthotropic plate [34].

3.2. Anisotropy

Soundboard anisotropy is a key parameter that quantifies the differences in elastic modulus along different directions of the soundboard, directly affecting the propagation characteristics of vibration energy and the uniformity of sound radiation. **Table 5** lists the anisotropy ratios of four types of soundboards, with T (tone-wood soundboard) having the highest ratio (4.59), L90 (laminate soundboard with vertical core) the lowest (3.68), and L180 (laminate soundboard with horizontal core) and L55 (laminate soundboard with incline core) falling in between.

Table 5. The relationship between the discrimination parameter and goodness of fit.

Sample group	Anisotropy	R^2
T	4.59	0.985
L90	3.68	0.735
L55	4.01	0.990
L180	4.25	0.937

It is worth noting that although the anisotropy of L55 (laminate soundboard with incline core) (4.01) is slightly smaller than that of T (tone-wood soundboard), the goodness of fit of its wave velocity–angle relationship (R^2 = 0.990) is slightly higher than that of T, indicating that through the inclined core laminate design, it is possible to achieve highly regular wave characteristics while maintaining moderate anisotropy. This finding suggests that the regularity of anisotropy may be more important than its strength: strong regularity in wave velocity variation implies high predictability of energy diffusion, which is beneficial for the uniformity design of the sound field. Conversely, although L90 (laminate soundboard with vertical core) has an anisotropy of 3.68, due to poor regularity, its actual acoustic performance may be unsatisfactory.

Considering both anisotropy and goodness-of-fit indicators, L55 shows the best overall performance among laminate soundboards: an anisotropy of 4.01, slightly lower than that of T, and an R^2 as high as 0.990, demonstrating strong regularity in its vibrations. This indicates that by optimizing the grain angles of the panels and the assembly method of the laminate, it is possible to achieve vibration characteristics in laminated structures that are close to those of T.

3.3. Broadband equivalent damping ratio

The exponential fitting method was employed to extract the envelope of the free-decay signal (**Figure 6**), from which the damping ratios at each tested angle were determined. The resulting data are tabulated in **Table 6**.

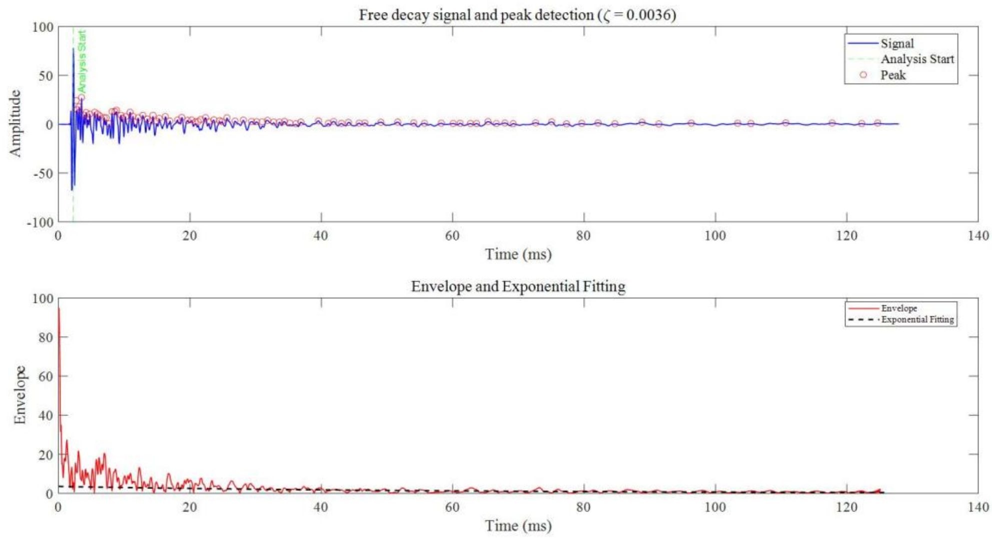

Figure 6. A schematic diagram of a free decay signal, its envelope, and the exponential fitting.

Table 6. Broadband damping ratios of the piano soundboards at different grain angles.

Angle α/°	T		L90		L55		L180	
	S1	S2	S1	S2	S1	S2	S1	S2
0	0.0031	0.0043	0.0028	0.0030	0.0047	0.0046	0.0027	0.0030
15	0.0022	0.0032	0.0047	0.0030	0.0041	0.0051	0.0040	0.0043
30	0.0040	0.0029	0.0042	0.0031	0.0040	0.0052	0.0041	0.0032
45	0.0043	0.0055	0.0039	0.0049	0.0037	0.0043	0.0040	0.0027
60	0.0039	0.0058	0.0033	0.0032	0.0051	0.0061	0.0040	0.0043
75	0.0049	0.0053	0.0027	0.0036	0.0050	0.0065	0.0029	0.0032
90	0.0053	0.0057	0.0026	0.0041	0.0054	0.0058	0.0062	0.0039

Note: S1 and S2 denote the two accelerometers. All values are broadband damping ratios.

From **Table 6**, it can be seen that the damping ratios of the four types of soundboards fluctuate with the angle α, but the amplitude and regularity of the fluctuations differ significantly. The damping ratio of T is approximately 0.0037 at 0°, decreases to about 0.0027 at 15°, and then generally increases with the angle, reaching 0.0055 at 90°. The slight decrease from 0° to 15° may be related to local material inhomogeneity or variations in measurement location, but the increasing trend from 15° to 90° agrees with the anisotropic damping behavior typical of natural spruce. As the grain angle increases, the transverse vibration components increase, frictional dissipation between fibers and cell walls is enhanced, and the damping ratio rises. Overall, the variation in the damping ratio of T reflects the anisotropy of natural wood, but it is not a strictly monotonic relationship; spatial variability is also embedded in the actual data.

The damping ratio of L90 does not change monotonically with the angle α; rather, there are two low-value regions at 0° and 60°–75°, and a high-value region at 15°–45°. This may be due to the coupling between the vertically laminated core and the face layer: when the measurement direction is close to the grain direction of the face layer (45°), the face layer dominates the vibration, and the shear dissipation of the adhesive layer increases; when the measurement direction is parallel to the grain direction of the core board (0°) or nearly perpendicular to the face layer (60°–75°), the continuous path of the core board prevails, or mode coupling reduces dissipation.

The damping ratio of L55 is lowest at 45° (0.00400) and highest at 75° (0.00575). This pattern originates from the 13° angle between the face layer (42°) and the core board (55°): when the measurement direction is nearly perpendicular to the face layer (around 75°), vibrations cross the fibers, resulting in high damping; at $\alpha = 45°$, interlayer shear is minimal, reducing damping. In addition, the damping ratios measured by S2 at α of 60° and 75° are significantly higher than those measured by S1, indicating that high damping is localized rather than uniform across the entire plate.

L180 has the lowest average damping ratio at $\alpha = 0°$ (0.00285). Apart from 0°, local peaks appear at 15° and 60°, which may be related to grain direction mismatches between the face layer and the core board. The elevated value at 90° mainly comes from the measurement by accelerometer S1, indicating that there is a strong local dissipation mechanism at this angle, while the value from accelerometer S2 is normal. Therefore, it cannot be simply concluded that L180 has high overall damping at 90°; the actual spatial non-uniformity is significant.

Looking at the overall data, the damping ratios of all soundboards are between 0.002 and 0.007. Among them, L55 (laminate soundboard with incline core) has the highest damping ratio, with an average of about 0.0051 and a maximum of 0.0065. T (tone-wood soundboard) exhibits an intermediate damping ratio, averaging 0.0040, reflecting the inherent damping characteristics of natural spruce, whose continuous fibers and uniform structure contribute to moderate energy dissipation. L180 (laminate soundboard with horizontal core) has a damping ratio slightly lower than that of T, averaging 0.0038. L90 (laminate soundboard with vertical core) has the lowest damping ratio, averaging only 0.0035, and its maximum (0.0049) is the lowest among the four soundboards.

The damping ratios of laminate soundboards with vertical and horizontal cores (L90 and L180) are both lower than those of the tone-wood soundboard (whose damping ratios range from 0.0022 to 0.0058), but their wave velocities are also lower than those of the tone-wood soundboard. This phenomenon reflects the decoupling of stiffness (wave velocity) and dissipation (damping ratio) mechanisms in composite structures [35–37]: although the presence of adhesive layers hinders the smooth transmission of vibrations, leading to a decrease in effective stiffness and a reduction in wave velocity [38], the adhesive layers do not generate significant additional energy dissipation through internal friction [39]. Instead, they may provide a more continuous transmission path across the interface for vibration waves, resulting in less energy loss during propagation and thus exhibiting a lower damping ratio than the tone-wood soundboard [39]. This indicates that in laminate soundboards, stiffness (wave velocity) and dissipation (damping ratio) are dominated by different mechanisms and no longer show a simple positive correlation.

It is worth noting that although L55 has the highest damping ratio, its goodness of fit of the wave velocity–angle relationship ($R^2 = 0.990$) is excellent, indicating a strong regularity in stiffness distribution, and the high damping ratio helps suppress unnecessary vibration ringing. L90 has the lowest damping ratio, but its wave velocity regularity is the worst ($R^2 = 0.735$), suggesting that while the structure contributes little to energy dissipation, it disrupts the directional regularity of wave propagation.

Therefore, in soundboard design, it is necessary to balance stiffness, regularity, and damping characteristics according to acoustic requirements.

It should be pointed out that the damping ratio obtained in this section by directly performing envelope fitting on the broadband signal is a composite value contributed by multiple modes, rather than the true damping ratio of a specific mode. Therefore, this result is only used for qualitative comparison of the overall trend of energy attenuation between the accelerometers.

3.4. Narrowband damping ratios

To investigate the impact of laminate splicing methods on the vibration energy spectrum distribution, a three-level wavelet packet decomposition was performed on signals from two accelerometers in the along-grain (0°) and across-grain (90°) directions for the four soundboards (tone-wood soundboard T, laminate soundboard with vertical core L90, laminate soundboard with incline core L55, laminate soundboard with horizontal core L180), resulting in 8 frequency band nodes (nodes 1–8). The average relative energy of each node was calculated, and the results are shown in **Figure 7**.

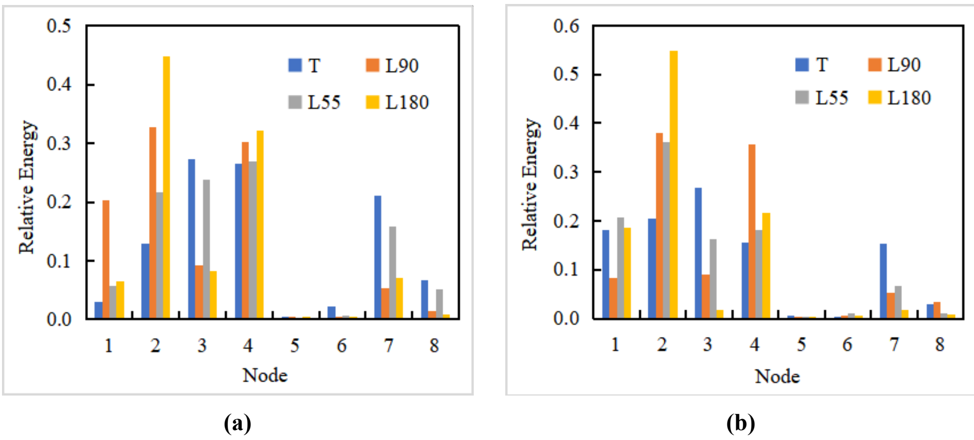

Figure 7. Relative energy comparison of wavelet packet nodes along and across the grain directions for the four soundboards: **(a)** Along the grain direction; **(b)** Across the grain direction.

As shown in **Figure 7**, the vibration energy of the four types of soundboards is mainly concentrated at nodes 1–4, corresponding to the 0–4,000 Hz frequency range. The energy proportions at nodes 5 and 6 (4,000–6,000 Hz) are extremely low (each < 1%), and those at nodes 7 and 8 (6,000–8,000 Hz) are also low. In other words, the collected vibration signals are mainly concentrated in the 0–4,000 Hz range.

This study uses a fourth-order Butterworth bandpass filter with a bandwidth set to 1% of the center frequency (i.e., $\Delta f = 0.01 f_{\mathrm{act,i}}$). To ensure zero phase distortion, the original signal is filtered bidirectionally using MATLAB's filtfilt function to obtain narrowband signals corresponding to each frequency (**Figure 8**). To investigate the frequency dependence of the damping ratio, four characteristic frequency points within this frequency range were selected for damping ratio calculation, and the results are shown in **Table 7**.

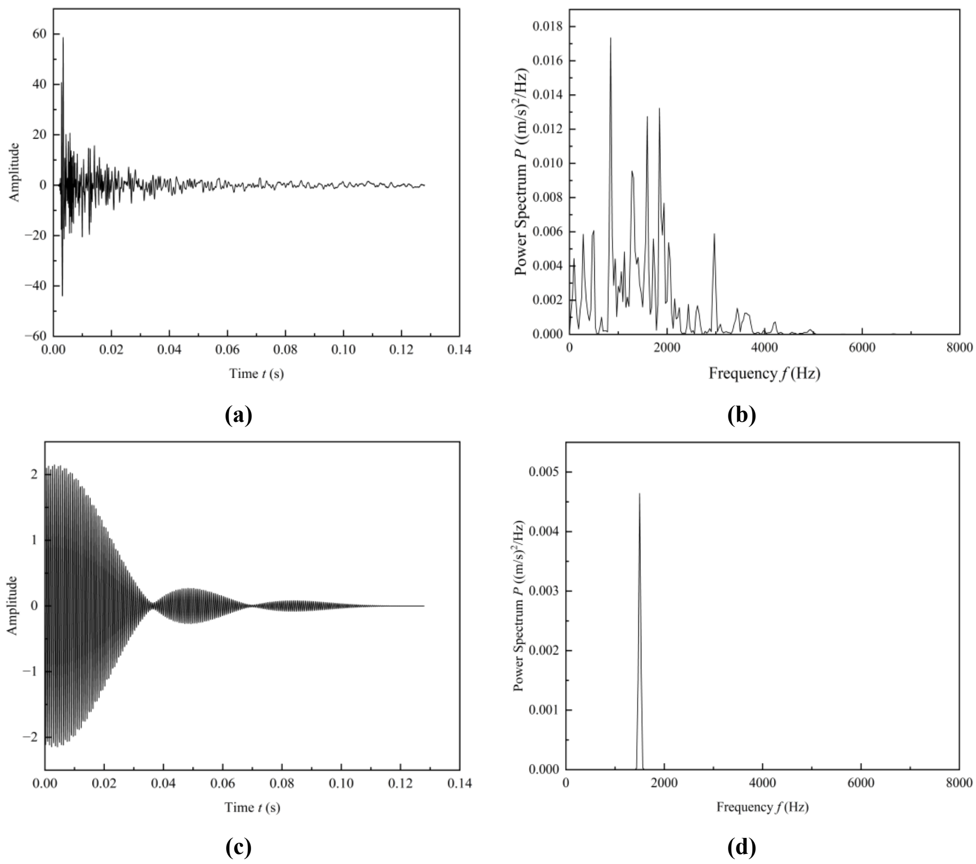

Figure 8. Original and narrowband-filtered signals at a center frequency of 1,500 Hz: **(a)** Time-domain waveform of the original signal; **(b)** Power spectrum of the original signal; **(c)** Time-domain waveform after narrowband filtering; **(d)** Power spectrum of the signal after narrowband filtering.

Table 7. Damping ratios of four types of piano soundboards at different frequencies.

Frequency/Hz	T	L90	L55	L180
500	0.0177	0.0167	0.0180	0.0178
1,500	0.0056	0.0056	0.0052	0.0047
2,500	0.0039	0.0041	0.0040	0.0040
3,500	0.0034	0.0033	0.0033	0.0037

As shown in **Table 7**, the damping ratios of the four soundboards exhibit significant frequency dependence in the 0–4,000 Hz range, with a consistent overall trend: the damping ratios gradually decrease as the frequency increases. In the 500–1,500 Hz range, the damping ratios are relatively high and decay rapidly; in the 1,500–3,500 Hz range, the downward trend of the curves gradually becomes more moderate. This phenomenon indicates that the vibration energy dissipation mechanisms of the four soundboards are dominated by frequency, and the damping characteristics tend to stabilize in the high-frequency region.

To describe the variation of the damping ratio with frequency, an exponential decay model $\zeta(f) = a \cdot e^{bf}$ is used for fitting (**Figure 9**), resulting in the model equations, Equations (12)–(15):

$$\text{T: } \zeta_1(f) = 0.02649e^{-0.0008563f}, \tag{12}$$

$$\text{L90: } \zeta_2(f) = 0.02417e^{-0.0007947f}, \tag{13}$$

$$\text{L55:}\ \zeta_3(f) = 0.02787e^{-0.0009218f}, \tag{14}$$

$$\text{L180:}\ \zeta_4(f) = 0.02771e^{-0.0009401f}, \tag{15}$$

where ζ is the damping ratio, f is the frequency, and a, b are constants obtained from the regression of the damping ratio against frequency.

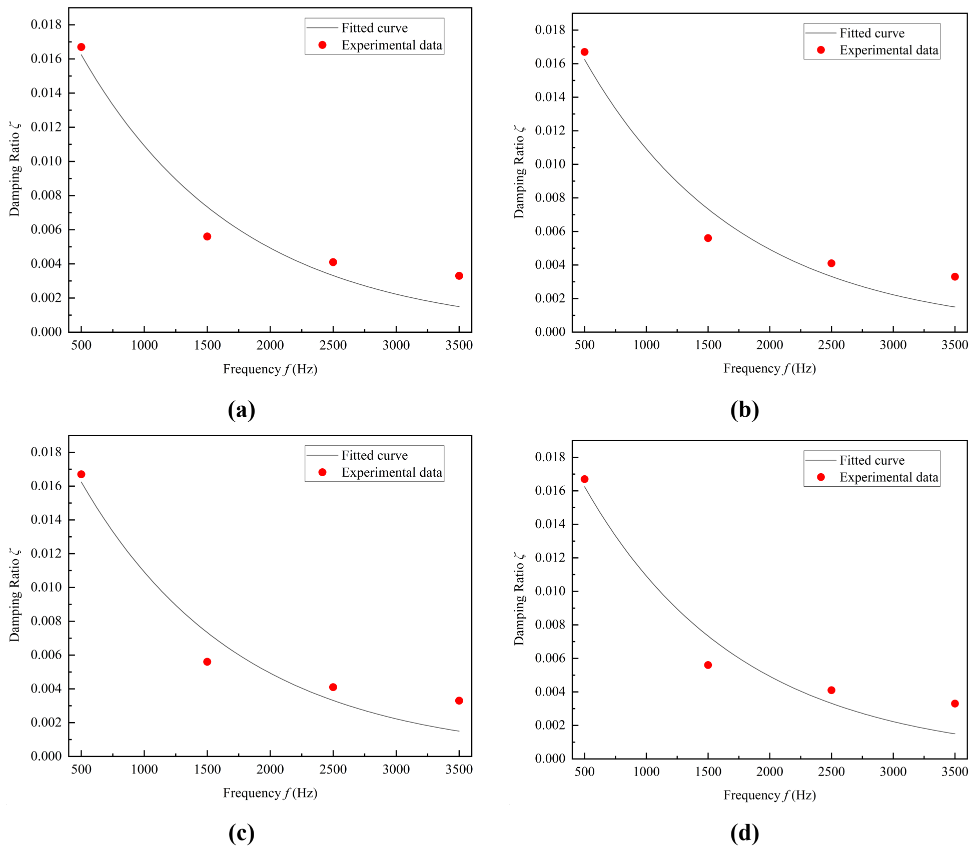

Figure 9. Damping ratio–frequency curves for the four soundboard types: **(a)** Tone-wood soundboard; **(b)** Laminate soundboard with vertical core; **(c)** Laminate soundboard with incline core; **(d)** Laminate soundboard with horizontal core.

As shown in **Table 8**, the R^2 values of the four types of soundboards all exceed 0.90, and the RMSE values are all below 0.0026, indicating that the exponential decay model can adequately describe the nonlinear relationship in which the damping ratio decreases with increasing frequency. This suggests that within the range of 0–4,000 Hz, the energy dissipation mechanisms of all soundboards have similar frequency-dominant characteristics.

Table 8. Root-mean-square error (RMSE) and coefficient of determination (R^2) for exponential decay fitting.

Sample group	**RMSE**	R^2
T	0.0020	0.941
L90	0.0019	0.940
L55	0.0022	0.933
L180	0.0026	0.904

The R^2 of T is 0.941, RMSE = 0.0020, indicating a relatively good fit, which shows that its damping ratio varies with frequency in a relatively clear and low-scatter manner, and the transmission and dissipation of vibration energy along the grain (0°) and across the grain (90°) directions are relatively stable. The R^2 of L90 is 0.940, RMSE = 0.0019, with a goodness of fit almost the same as that of T and the lowest RMSE. This indicates that although L90 is insensitive to the propagation direction (weak wave velocity anisotropy), its frequency-dependent damping ratio is very regular, possibly because the vertical lamination structure restricts interlayer shear deformation. Under vibration excitation at different frequencies, the main physical process of vibration energy dissipation is the same, without giving rise to additional dissipation mechanisms or fluctuations with frequency. The R^2 of L55 is 0.933, RMSE = 0.0022, slightly lower than that of T and L90 but still good. This is due to the small angle difference between the face layer and core board (42°/55°), which causes interlayer shear coupling and wave mode conversion, leading to minor fluctuations in the damping ratio at certain frequencies, slightly increasing the fitting residuals. Although its overall anisotropy is lower than that of T, interlayer coupling effects disrupt the smoothness of the damping ratio-frequency curve, causing fluctuations at some frequencies; however, the overall exponential decay trend remains significant. The R^2 of L180 is 0.904, RMSE = 0.0026, with the lowest goodness of fit, possibly due to local mode coupling or interlayer slip in the horizontal lamination structure, causing the damping ratio in some frequency bands to deviate from the ideal exponential decay curve, thereby increasing the fitting residuals.

4. Conclusion

This study used the free vibration method and, based on synchronized data acquired by two accelerometers, systematically analyzed the time-domain vibration wave characteristics of four types of piano soundboards (T (tone-wood soundboard), L90 (laminate soundboard with vertical core), L55 (laminate soundboard with incline core), and L180 (laminate soundboard with horizontal core)). Through wavefront identification, wave velocity calculation, evaluation of anisotropy, and damping characteristic analysis, this study clarified the differences and variation patterns of the four soundboards in terms of wave velocity, anisotropy, and damping ratio, revealed the mechanism by which laminated structures affect the regularity of wave velocity, the degree of anisotropy, and the frequency dependence of damping, and drew the following main conclusions:

(1) For all soundboards, the wave velocity along the grain direction (0°) is significantly higher than that across the grain direction (90°), and the wave velocities of T at all measured angles are higher than those of the three laminate soundboards. Polynomial fitting of the wave velocity–grain angle relationship for soundboards shows that T and L55 exhibit the most significant regularity in wave velocity variation with angle, with R^2 values of 0.985 and 0.990, respectively; L180 shows good regularity (0.937) but has local fluctuations; L90 has poor regularity (0.735). This indicates that the ranking of wave velocity regularity for the four soundboards is: L55 > T > L180 > L90.

(2) The anisotropy of the four soundboards is calculated, yielding 4.59 for T, 3.68 for

L90, 4.01 for L55, and 4.25 for L180, indicating that the degree of anisotropy of the four soundboards is: T > L180 > L55 > L90.

(3) Using an envelope fitting method based on the Hilbert transform, the damping ratio of each soundboard was extracted from the free decay signals. The damping ratio of T ranges from 0.0022 to 0.0058; that of L90 ranges from 0.0026 to 0.0049, with its upper limit significantly lower than those of the other three; that of L55 ranges from 0.0037 to 0.0065; that of L180 ranges from 0.0027 to 0.0062, close to the range of T.

(4) By calculating the relative node energy of the vibration signal, it is found that the signal is mainly concentrated in the 0–4,000 Hz range. The damping ratios of the four soundboards exhibit a consistent overall trend within this frequency band: the damping ratios gradually decrease with increasing frequency. Moreover, the damping ratios are relatively high and decay quickly in the 500–1,500 Hz range, while the downward trend gradually moderates in the 1,500–3,500 Hz range.

In summary, although the equivalent damping ratios of the four types of soundboards differed within a certain range, their average damping ratios were close. The wave velocity and anisotropy of the tone-wood soundboard are significantly higher than those of the three laminate soundboards. Among the laminate soundboards, L55 is significantly superior to L90 and L180 in both wave velocity and regularity. Consequently, the comprehensive performance ranking of the four soundboards is: T > L55 > L180 > L90.

Although this study achieved certain results, there were still some limitations. Firstly, the frequency analysis was limited to the 0–4,000 Hz range, and modal behavior at higher frequencies was not explored. Secondly, the experiments were conducted under standard laboratory conditions (temperature and humidity), so the environmental stability of the laminate soundboards remains unclear. In addition, although anisotropy and damping ratios were derived from wave propagation and free decay signals, no direct mechanical or acoustic performance tests were conducted to relate these characteristics to actual musical instrument applications.

To address these limitations, future research should focus on the following aspects. On one hand, pulse excitation or shaker excitation should be used to extend the frequency range beyond 4,000 Hz. On the other hand, the effects of humidity and temperature cycling on wave velocity, anisotropy, and damping should be evaluated, and the measured vibration characteristics should be correlated with acoustic output parameters. Furthermore, future work should further link these measured parameters to tonal quality through perceptual evaluation, thereby strengthening the practical relevance of the findings.

Author contributions: Conceptualization, JC and ZL; methodology, JC, ZL and GW; software, JC; validation, JC and GW; formal analysis, JZ and LH; investigation, JC, HC and LH; resources, JC and JZ; data curation, JC; writing—original draft preparation, JC; writing—review and editing, JC, JZ and GW; visualization, JC; supervision, ZL; project administration, ZL; funding acquisition, ZL. All authors have read and agreed to the published version of the manuscript.

Funding: This research was funded by the National Natural Science Foundation of China, grant numbers 32271781.

Institutional review board statement: Not applicable.

Informed consent statement: Not applicable.

Data availability statement: The data that support the findings of this study are available from the first author and corresponding author upon reasonable request.

Conflict of interest: The authors declare no conflict of interest.

AI use statement: During the preparation of this work, the authors used DeepSeek for language polishing. The authors subsequently reviewed and edited the content as necessary and take full responsibility for the final content of the published article.

References

1. Bal BC, Bektaş İ. The effects of wood species, load direction, and adhesives on bending properties of laminated veneer lumber. BioResources. 2012; 7(3): 3104–3112. doi: 10.15376/biores.7.3.3104-3112
2. Liu Z, Liu Y, Miao Y, et al. Relationship between vibration property of resonance board and subjective evaluation of piano acoustical quality. Scientia Silvae Sinicae. 2009; 45(4): 100–106. Available online: https://html.rhhz.net/linyekexue/html/090417.htm (in Chinese)
3. Xu H, Xu G, Wang L, et al. Propagation behavior of acoustic wave in wood. Journal of Forestry Research. 2014; 25(3): 671–676. doi: 10.1007/s11676-014-0506-6
4. Guo J, Fang S, Li M, et al. Anisotropic study of wave velocity and energy decay of stress wave propagation on wood surface. Wood Material Science & Engineering. 2025; 1–10. doi: 10.1080/17480272.2025.2589486
5. Bader R, Plath N. Impact of Damping on Oscillation Patterns on the Plain Piano Soundboard. Acoustics. 2022; 4(4): 1013–1027. doi: 10.3390/acoustics4040062
6. Yang Y. Research on GRNN Prediction Model for Acoustic Quality of Yueqin Based on Wood Vibration Characteristics. Forest Engineering. 2024; 40(4): 160–167. Available online: https://cjournal.hep.com.cn/1006-8023/CN/10.7525/j.issn.1006-8023.2024.04.017 (in Chinese)
7. Sanabria SJ, Furrer R, Neuenschwander J, et al. Analytical modeling, finite-difference simulation and experimental validation of air-coupled ultrasound beam refraction and damping through timber laminates, with application to non-destructive testing. Ultrasonics. 2015; 63: 65–85. doi: 10.1016/j.ultras.2015.06.013
8. Brémaud I, Gril J. Moisture content dependence of anisotropic vibrational properties of wood at quasi equilibrium: analytical review and multi-trajectories experiments. Holzforschung. 2021; 75(4): 313–327. doi: 10.1515/hf-2020-0028
9. Faktorová D, Stanciu MD, Krbata M, et al. Analysis of the Anisotropy of Sound Propagation Velocity in Thin Wooden Plates Using Lamb Waves. Polymers. 2024; 16(6): 753. doi: 10.3390/polym16060753
10. Vallely S, Schoenwald S. Higher-order modal parameter estimation and verification of cross-laminated timber plates for structural-acoustic analyses. Acta Acustica. 2024; 8: 52. doi: 10.1051/aacus/2024043
11. Nkibeu JB, Makomra V, Sali M, et al. Damping properties of some tropical wood species determined by free transverse vibration method. Wood Material Science & Engineering. 2025; 20(6): 1189–1195. doi: 10.1080/17480272.2024.2388213
12. Liu Y, Zhao G. Wood Science, 2nd ed. China Forestry Publishing House; 2012.
13. Song R, Li Y, Han S, et al. Mechanism by Which Heat Treatment Influences the Acoustic Vibration Characteristics of Bamboo. Materials. 2025; 18(23): 5335. doi: 10.3390/ma18235335
14. Cai B, Bo L, Campbell A, et al. Noncontact pulsed laser-scanning laser Doppler vibrometer (PL-SLDV) phased array imaging for damage detection in composites. Ultrasonics. 2026; 157: 107787. doi: 10.1016/j.ultras.2025.107787
15. Shi J, Yin S, Huang W, et al. Application of vibrational methods in wood performance testing: A short review. BioResources. 2025; 20(2). doi: 10.15376/biores.20.2.Shi
16. Urgela S. Grading of wooden plates for musical instrument making by means of holographic interferometry. Optical

Engineering. 1998; 37(7): 2108. doi: 10.1117/1.601702
17. Zhang C, Luo J, Xu W, et al. Comparison of two kinds of sound velocity measurement methods of spruce timber used for piano. Journal of Forestry Engineering. 2010; 24(3): 56–59. (in Chinese)
18. Stanciu MD, Nastac SM, Chen CW, et al. Exploring the Dynamic Properties of Tropical and Temperate Wood Species for Musical Instruments. Applied Sciences. 2025; 15(22): 11926. doi: 10.3390/app152211926
19. Kouroussis G, Fekih LB, Descamps T. Using experimental modal analysis to assess the behaviour of timber elements. Mechanics & Industry. 2017; 18(7): 704. doi: 10.1051/meca/2017042
20. Ege K, Boutillon X, Rébillat M. Vibroacoustics of the piano soundboard: (Non)linearity and modal properties in the low- and mid-frequency ranges. Journal of Sound and Vibration. 2013; 332(5): 1288–1305. doi: 10.1016/j.jsv.2012.10.012
21. Zhao K, Yang Y, Luo Y. Broadband Love Wave Phase Velocity Maps Based on Modified Double-Beamforming of Ambient Noise Cross-Correlations. Journal of Geophysical Research: Solid Earth. 2024; 129(3). doi: 10.1029/2023JB026871
22. Li M, Wang M, Ding R, et al. Study of acoustic emission propagation characteristics and energy attenuation of surface transverse wave and internal longitudinal wave of wood. Wood Science and Technology. 2021; 55(6): 1619–1637. doi: 10.1007/s00226-021-01329-y
23. Bahmani H, Mostafaei H, Mostofinejad D. Review of Energy Dissipation Mechanisms in Concrete: Role of Advanced Materials, Mix Design, and Curing Conditions. Sustainability. 2025; 17(15): 6723. doi: 10.3390/su17156723
24. Hu Z, Wang X, Zheng G. Free Vibration Identification of the Geometrically Nonlinear Isolator with Elastic Rings by Using Hilbert Transform. In: Nonlinear Dynamics, Volume 1. Springer International Publishing; 2017. pp. 69–76. doi: 10.1007/978-3-319-54404-5_7
25. Thomson WT. Theory of Vibration with Applications, 4th ed. CRC Press; 1993. doi: 10.1201/9780203718841
26. Xu Z, Tao Y, Hernandez L. Novel Methods for the Computation of Small-Strain Damping Ratios of Soils from Cyclic Torsional Shear and Free-Vibration Decay Testing. Geotechnics. 2021; 1(2): 330–346. doi: 10.3390/geotechnics1020016
27. Merhar M. Identification of Damping of Spruce Wood (Picea abies) under Various Levels of Moisture Content Using Time-Scale Decomposition. Polymers. 2024; 16(10): 1313. doi: 10.3390/polym16101313
28. Wavelet Packets: Decomposing the Details. Available online: https://ww2.mathworks.cn/help/wavelet/ug/wavelet-packets-decomposing-the-details.html (accessed on 25 April 2026).
29. Horbelt N, Dunlop JWC, Bertinetti L, et al. Effects of moisture and cellulose fibril angle on the tensile properties of native single Norway spruce wood fibres. Wood Science and Technology. 2021; 55(5): 1305–1318. doi: 10.1007/s00226-021-01315-4
30. He L, Liang Y, Zhang L, et al. Measurement and Analysis of the Vibration Responses of Piano Soundboards with Different Structures. Materials. 2024; 17(5): 1004. doi: 10.3390/ma17051004
31. Tan C, Huang B, Liu D, et al. Effect of Mimic Vegetation with Different Stiffness on Regular Wave Propagation and Turbulence. Water. 2019; 11(1): 109. doi: 10.3390/w11010109
32. Gupta S, Haq M, Cvetkovic K, et al. Numerical Far-Field Investigation into Guided Waves Interaction at Weak Interfaces in Hybrid Composites. Journal of Composites Science. 2025; 9(8): 387. doi: 10.3390/jcs9080387
33. Wang L, Rokhlin SI. Ultrasonic wave interaction with multidirectional composites: Modeling and experiment. The Journal of the Acoustical Society of America. 2003; 114(5): 2582–2595. doi: 10.1121/1.1616920
34. Ye J, Sun Y. Sound Radiation Characteristics Analysis of Laminates Based on Sound Radiation Modal Method. Noise and Vibration Control, 2023; 43(3): 27–33. Available online: https://nvc.sjtu.edu.cn/CN/abstract/abstract3466.shtml (in Chinese)
35. Shan S, Zhang Y, Song Y, et al. Cumulative second harmonic Lamb wave generation and propagation in composite laminates: an insight into the influence of material anisotropy and damping. e-Journal of Nondestructive Testing. 2024; 29(7). doi: 10.58286/29758
36. Feng H, Li L. Review of damping composite materials and structures involving self-healing constituents. Frontiers of Mechanical Engineering. 2025; 20(2): 15. doi: 10.1007/s11465-025-0833-7
37. Al-Dulaijan SU, Youzera H, Meftah SA, et al. Nonlinear Damping and Vibration Assessment of Sandwich Beam with Composite Faces and Viscoelastic Core Layer. International Journal of Structural Stability and Dynamics. 2024; 24(08): 2450083. doi: 10.1142/S0219455424500834

38. Li Z, Chu S, Zhang Y, et al. Transforming interface properties of wood laminate composites functionalized by adhesive penetration. Composites Part B: Engineering. 2023; 263: 110859. doi: 10.1016/j.compositesb.2023.110859
39. Chełmecki J, Szeptyński P, Jasińska D, et al. Analyzing the Vibration Response of Adhesively Bonded Composite Cantilevers. Materials. 2024; 18(1): 93. doi: 10.3390/ma18010093